SAND2015-8941C

A Modal Model to Simulate Typical Structural Dynamic Nonlinearity

Randall L. Mayes
Benjamin R. Pacini
Structural Dynamics X-ray/NDE Department
Sandia National Laboratories*
P.O. Box 5800 - MS0557
Albuquerque, NM, 87185
rlmayes@sandia.gov
brpacin@sandia.gov

Daniel R. Roettgen
University of Wisconsin - Madison
Engineering Mechanics Department
droettgen@wisc.edu

Nomenclature

FRF	frequency response function
dof	degree of freedom
sdof	single degree of freedom
c	damping coefficient
$d(t)$	decay function for damping as function of time
k	stiffness coefficient
t	time
x	physical displacement dof
q	modal dof
ζ	modal damping ratio
ω	frequency in radians per second
A	amplitude
F	force
f	frequency in cycles/sec
K_∞	linear stiffness for Iwan model
$\mathbf{H}$	frequency response function matrix
$\mathbf{P}$	modal response matrix
$\mathbf{U}$	known force vector
$\mathbf{W}$	weighting matrix
Q	analytic signal created with use of Hilbert transform
$\mathcal{H}$	Hilbert transform
$\theta(t)$	phase as a function of time
χ	Iwan parameter related to power law damping
$\overline{\boldsymbol{\Psi}}$	modal filter vector
$\boldsymbol{\Phi}$	mode shape matrix
d	subscript for damped
lin	subscript for linear
n	subscript for natural
nl	subscript for nonlinear
$\mathcal{F}$	subscript for Fourier transform
$+$	superscript indicating the Moore-Penrose pseudo-inverse of a matrix

*Sandia National Laboratories is a multi-program laboratory managed and operated by Sandia Corporation, a wholly owned subsidiary of Lockheed Martin Corporation, for the U.S. Department of Energy National Nuclear Security Administration under Contract DE-AC04-94AL85000.

1 Abstract
Some initial investigations have been published which simulate nonlinear response with almost traditional modal models: instead of connecting the modal mass to ground through the traditional spring and damper, a nonlinear Iwan element was added. This assumes that the mode shapes do not change with amplitude and there are no interactions between modal degrees of freedom. This work expands on these previous studies. An impact experiment is performed on a structure which exhibits typical structural dynamic nonlinear response, i.e. weak frequency dependence and strong damping dependence on the amplitude of vibration. Use of low level modal test results in combination with high level impacts are processed using various combinations of modal filtering, the Hilbert Transform and band-pass filtering to develop response data that are then fit with various nonlinear elements to create a nonlinear pseudo-modal model. Simulations of forced response are compared with high level experimental data for various nonlinear element assumptions.

Keywords – Nonlinear System Identification, Nonlinear Simulation, Structural Dynamics, Modal Model

2 Introduction and Motivation
A large class of structural dynamic system responses are mildly nonlinear in stiffness (a few percent modal frequency change) and significantly nonlinear in damping (hundreds of percent damping ratio change) as a function of amplitude of vibration. We desire to experimentally test in a way to identify such a system and then simulate the nonlinear response analytically. Such systems will typically be linear at low level excitation. At higher levels of excitation the resonant frequencies typically decrease slightly and the apparent damping can increase up to 300 percent. Structures with joints typically have this softening behavior. Low linear models used to simulate the response may over-predict the nonlinear response by tens to hundreds of percent. Consider a frequency response function (FRF) from the hardware used in this work due to a high level and a low level impact as shown in Figure 1. The low level FRF peak is almost a factor of two greater than the high level FRF peak. Occasionally the resonant frequency will go up slightly and the apparent damping will go down with an increase in the amplitude. We desire to be able to simulate both softening and stiffening behavior. Segalman[1] explored the possibility of utilizing a modal Iwan approach to capture spatially distributed nonlinear energy dissipation with a two degree-of-freedom (dof) analytical model. Deaner[2] fleshed out the concept with a nonlinear beam model, and with jointed beam hardware. He used a modal approach with a four parameter Iwan element in parallel with a linear spring and damper to achieve a satisfactory simulation. We expand on his approach.

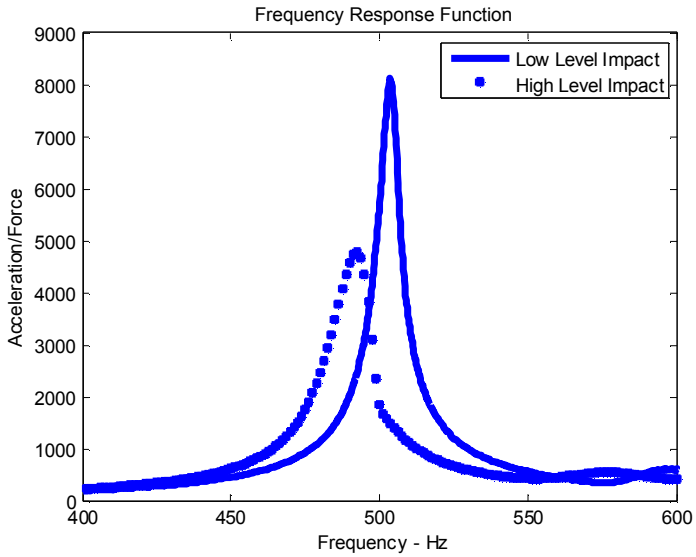

Figure 1 - Drive Point FRF magnitude - low level vs high level impact force

The approach utilizes a pseudo-modal model. We assume that a superposition of the modal responses can be multiplied by the mode shape matrix to estimate the response at physical dof. Inherent in this approach is the assumption that the mode shapes do not change with response amplitude, and that the modal dof do not interact. Our approach begins with the standard modal model using a linear spring and damper for each modal mass. The spring and damper are identified in a standard low-level modal impact test. Then we assume that nonlinear elements can be connected in parallel with the standard linear elements. A high level impact test on the nonlinear structure provides data for fitting the nonlinear parameters. Three different nonlinear elements were examined in this work: 1. a four parameter Iwan in parallel with a linear stiffness and damper; 2. Feldman's FREEVIB stiffness and damping; and 3. cubic polynomials of stiffness and damping as a function of response amplitude. We set these models on approximately the same footing by identifying six parameters in each model for

each mode of vibration. After the elements were identified, we simulated a high level structural response and propagated the modal responses to all the measured dof and compared simulations to measured responses. A key portion of the success of this approach comes from a modal filter that can filter out all the modal responses of the structure except the single mode of interest. The single dof modal filtered response is used to identify the nonlinear parameters. The Iwan and Feldman models also require that the Hilbert Transform of the modal response be computed as a step in the identification process. The cubic stiffness/damping model does not have this requirement.

In Section 3 the test hardware and instrumentation is described along with the test approach. Signal preprocessing of modal filters, band-pass filters and the Hilbert Transform is presented in Section 4. Section 5 describes the three nonlinear modeling options and their parameter identification processes. In Section 6 the simulation results are compared against measured high level data, and observations associated with each model are given. Section 7 provides conclusions.

3 Experiment

3.1 Hardware Description

A solid model cross-section of the test hardware chosen for this analysis is shown in Figure 2 and some of the physical hardware is shown in Figure 3. The foam, mass, and compression plate are placed in the cylinder and a hydraulic press is used to compress these internals to a specified pre-load as measured by three load cells mounted on the mass. The threaded ring is then screwed in to hold the assembly together. The plate-beam is then mounted on the forward face of the cylinder using eight bolts. The cylinder and plate-beam are 6061 T6 aluminum, the rigid urethane foam is Coastal Enterprises PBLT-20 nominal 20 pound/ft^3, and the mass is steel.

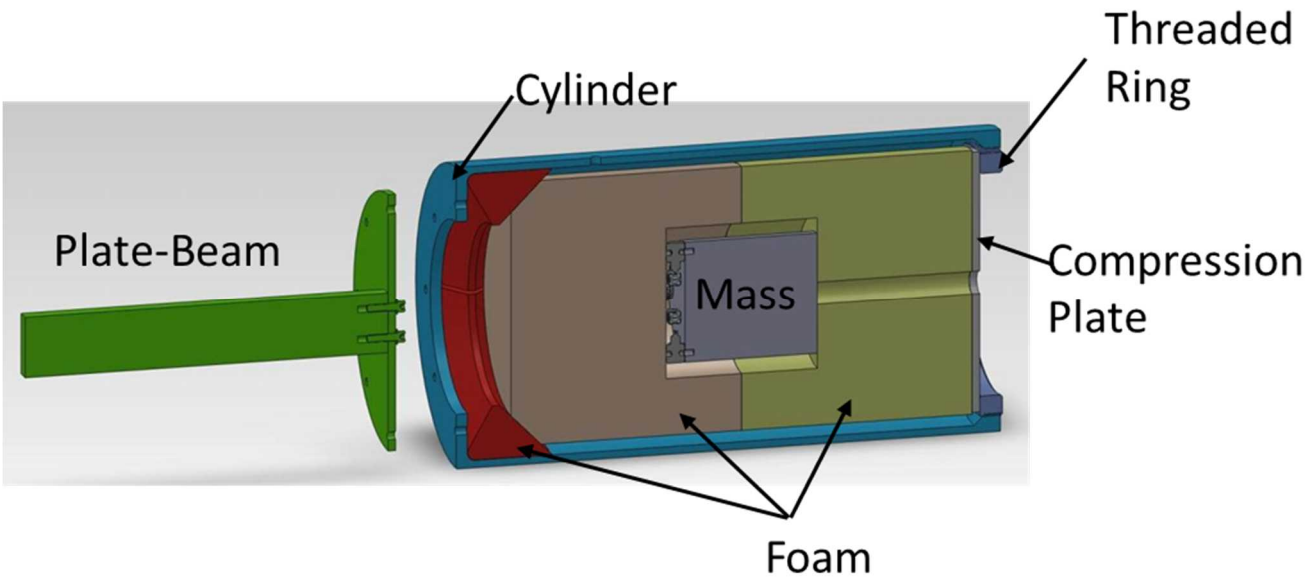

Figure 2 - Full system solid model

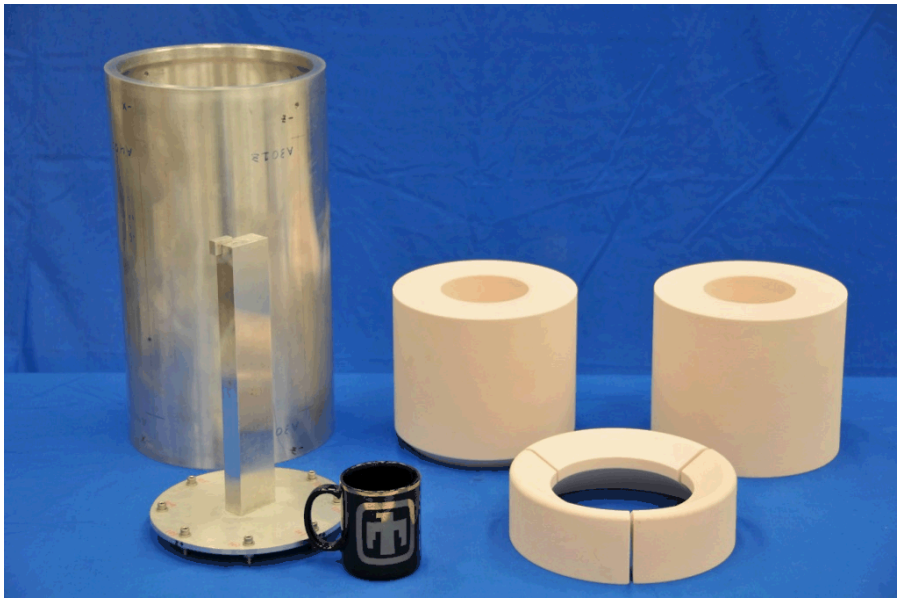

Figure 3 - Physical test hardware

3.2 Test Set-Up

The test hardware shown in Figure 4 was softly suspended using two bungee cords to approximate a free-free boundary condition and instrumented with 100 mV/g accelerometers. External triaxial accelerometers were mounted at 15 locations shown in Figure 5. The internal mass was instrumented with 10 accelerometer channels to capture its rigid body motion.

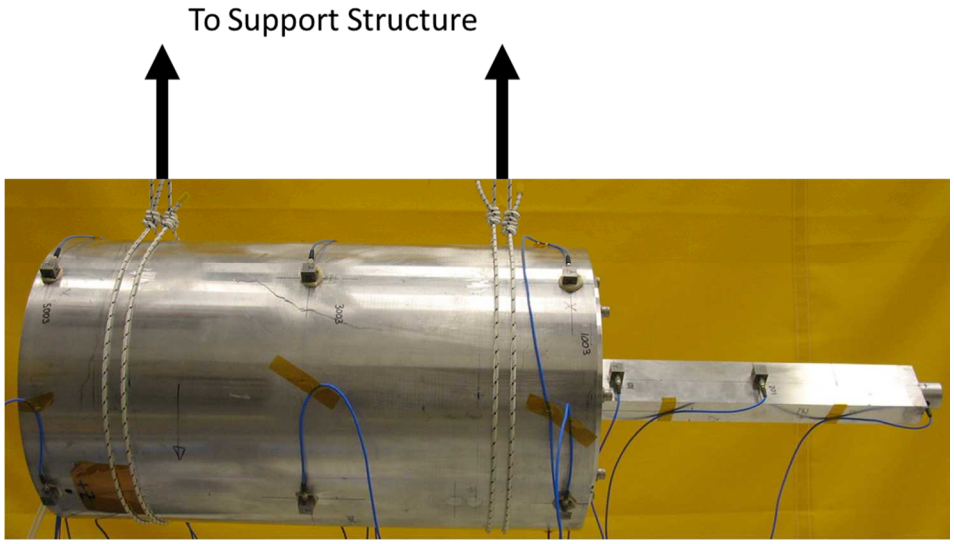

Figure 4 - Test hardware suspension

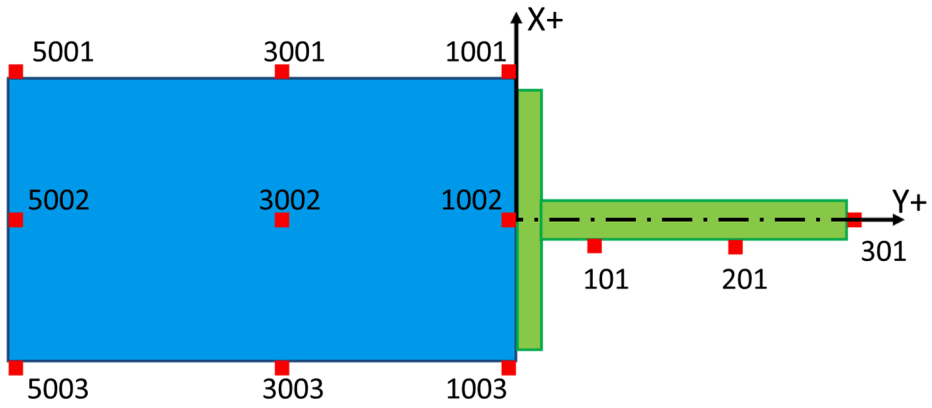

Figure 5 - External geometry, side view

Two series of hammer impact tests were conducted on the hardware described above. The first minimized the nonlinear response by applying low level inputs with peak forces of approximately 23 N at the three locations shown in Table 1. These data were used to extract parameters for the linear modal model of the hardware. The second set of tests excited nonlinearities with inputs at these same locations but with much higher peak forces: 180 and 400 N for the radial and axial hits, respectively. 400 N was not used for the radial inputs because this force level over-ranged the drive point accelerometers. The high level data was used to first identify which modes were nonlinear (see Section 3.3) and secondly to extract parameters for the nonlinear models discussed in Section 5.

Table 1 - Excitation Information

Input DOF	Description	Low Level Peak Force (N)	High Level Peak Force (N)
301Y-	Axial input at tip of beam	23	400
5002R-	Radial input at aft end of can in the stiff direction of the beam	23	180
5003R-	Radial input at aft end of can in the soft direction of the beam	23	180

3.3 Preliminary Modal Results

The Synthesize Modes And Correlate (SMAC) program by Mayes and Hensley [3] was used to extract two sets of modal parameters from the low and high level impact data using a real modes approximation in Table 2. Rigid body mode shapes were calculated from solid model mass properties.

Table 2 - Linear Modal Parameters[1,2]

Mode	Low Level		High Level		Δf_n (%)	$\Delta\zeta$ (%)	Reference	Shape Description
	f_n (Hz)	ζ (%cr)	f_n (Hz)	ζ (%cr)				
7	119	0.36	116	0.95	-3	167	5003R-	1st beam bend in X
8	160	0.21	158	0.60	-1	190	5002R-	1st beam bend in Z
9	276	2.46	273	3.60	-1	46	5002R-	Torsion of internal mass
10	282	2.10	280	1.92	-1	-9	5003R-	Translation in X of internal mass
11	302	2.34	298	2.40	-1	3	5002R-	Internal mass off-axis twist
12	503	0.67	491	1.23	-3	84	301Y-	Axial mode of beam Y
13	592	2.02	570	2.91	-4	44	301Y-	Rotation of internal mass about Z
14	635	2.00	630	2.27	-1	14	5002R-	Rotation of internal mass about X
15	699	1.26	692	1.44	-1	14	301Y-	Axial mode of internal mass Y
16	734	1.27	732	1.38	0	9	5003R-	Foam mode X
17	759	1.13	758	1.16	0	3	5002R-	Foam mode Z

[1]Modes highlighted in green were considered nonlinear

[2]Rigid body modes not shown.

The low level modal parameters were used to create the linear modal model used in the later sections of this report.

The high level modal parameters were used to determine which modes should be modeled as nonlinear. Since damping values extracted from measured data can have 10% uncertainty, the heuristic used in this work was that any mode with a damping shift of greater than 30% was declared nonlinear. Modes 7-9, 12, and 13 were thus selected to be modeled as nonlinear.

4 Signal Processing

To develop a nonlinear modal model, our approach requires the structural response be separated into the individual modal responses. This requires some type of filter that can transform multiple sensor measurements into modal coordinates. Once these modal responses are calculated, further processing is required to aid nonlinear parameter identification. The following sections detail this two-step procedure. Section 4.1 describes three different types of modal filters, discusses the advantages and disadvantages of each, and concludes by selecting the modal filter used for this work. Section 4.2 discusses band-pass filtering and the Hilbert Transform which are then used to extract frequency and damping information from the modally filtered data that will be later used to calculate parameters for two nonlinear models.

4.1 Modal Filtering

This section describes three modal filters that can be used to transform measurements in physical coordinates to modal responses. We desire a modal filter such that

$$\overline{\boldsymbol{\Psi}}^T \overline{\mathbf{x}} = q_i \tag{1}$$

where q_i is the i^{th} modal dof, column vector $\overline{\mathbf{x}}$ contains measured responses, and $\overline{\boldsymbol{\Psi}}$ is the vector of weights transforming the measured responses to the modal response. Three modal filters are investigated.

4.1.1 SMAC Modal Filter

The SMAC modal filter[4] operates directly on the FRFs. If one operates on (1) in the frequency domain and divides by the input force, then

$$\overline{\boldsymbol{\Psi}}^T \overline{\mathbf{H}}_x = H_{qi} \tag{2}$$

where $\mathbf{H}_x$ is now a vector of measured FRFs and H_{qi} is an analytically calculated single dof (sdof) FRF with frequency and damping as extracted from the high level impact data. Columns for every frequency line are added to $\mathbf{H}_x$ and H_{qi} creating a matrix of $\mathbf{H}_x$ and a vector of the analytical FRF $\mathbf{H}_{qi}$. Transposing and isolating the modal filter on the left side yields

$$\overline{\boldsymbol{\Psi}} = \mathbf{H}_x^{T+} \overline{\mathbf{H}}_{qi}^T \tag{3}$$

where the superscript $^+$ represents the pseudo-inverse. Hence, the SMAC modal filter is obtained with the measured FRFs and an analytical sdof FRF constructed using the extracted frequency and damping from the high level linear modal parameter extraction.

4.1.2 Full Modal Filter

We denote the Full Modal Filter (FMF) as one derived from extracted mode shapes. The modal substitution can be written as

$$\overline{\mathbf{x}} = \boldsymbol{\Phi} \overline{\mathbf{q}} \tag{4}$$

where $\boldsymbol{\Phi}$ is a matrix of all rigid body and elastic extracted mode shapes in the frequency band. By pre-multiplying by the pseudo-inverse of the mode shape matrix one obtains

$$\boldsymbol{\Phi}^+ \overline{\mathbf{x}} = \overline{\mathbf{q}} \tag{5}$$

so one can recognize the set of all modal filters in the $\boldsymbol{\Psi}$ matrix as

$$\boldsymbol{\Psi}^T = \boldsymbol{\Phi}^+ \tag{6}$$

Thus the full modal filter is derived from extracted mode shapes and rigid body mode shapes. In this work, the elastic mode shapes were extracted from the low level impact data.

4.1.3 Single Modal Filter

The single modal filter (SMF) was derived using only one mode shape in (5) as

$$\overline{\boldsymbol{\Phi}}_i^+ \overline{\mathbf{x}} = q_i \tag{7}$$

so that

$$\overline{\boldsymbol{\Psi}}_i^T = \overline{\boldsymbol{\Phi}}_i^+ \tag{8}$$

The FMF and SMAC modal filters inherently suppress the response of all modes but one. However, the SMF does not, so it relies on the frequency being isolated and band-pass filtering to suppress other modes.

4.1.4 Modal Filter Results and Comparison

All three modal filters were evaluated for each mode extracted from the experimental system. Consider the results for mode 13 at about 590 Hz shown in Figure 6. Neither the SMF or FMF can remove the effects of the 491 Hz axial mode like the SMAC modal filter.

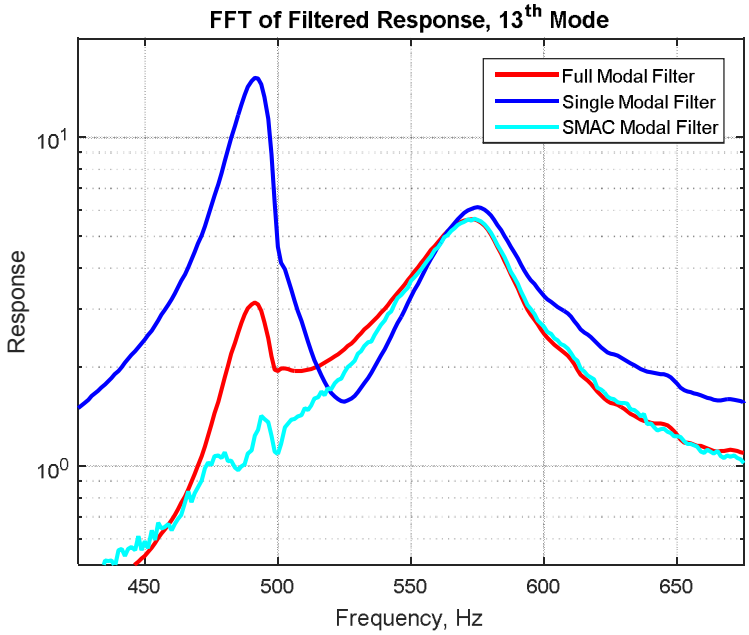

Figure 6 - Modal filter results for mode 13 at 592 Hz

However, the SMAC modal filter does not always perform better. Consider the modal filter results for mode 9 at 273 Hz in Figure 7. Notice the small shoulder in the SMAC modal filter result (cyan) at 282 Hz. The 282 Hz mode was not removed as well with the SMAC modal filter as with the other two. Note that all three modal filters failed to get rid of the mode at 302Hz. The effects of these contaminating peaks will be discussed in later sections of this work.

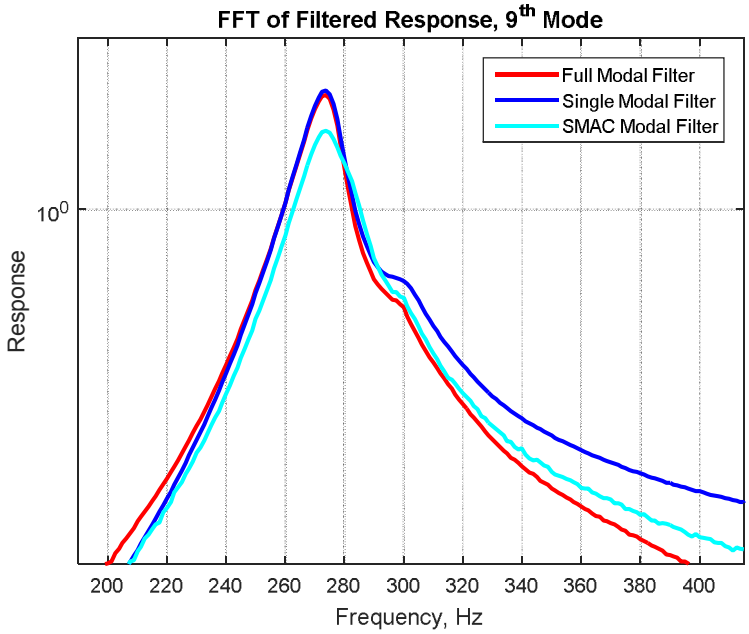

Figure 7 – Modal filter comparison mode 9

Although it did not perform better for every single mode, the SMAC modal filter generally suppressed all other modes besides the one desired better than the FMF and SMF, so it was chosen for this work.

4.2 Hilbert Transform and Band-pass Sensitivity

Once we have obtained a single degree of freedom response from a combination of modal and band-pass filtering, two of the nonlinear methods require quantifying the damping and frequency as a function of response amplitude. The procedure for accomplishing this closely follows the work from [5] and [6]. In this work, the Hilbert Transform is computed and a cubic polynomial is fit to the time varying amplitude and phase. This approach fits the modal impulse response, $\ddot{q}(t)$, to the following functional form,

$$\ddot{q}(t) = e^{d(t)}\cos[\theta(t)] \tag{9}$$

where $d(t)$ and $\theta(t)$ are each cubic polynomials in time and are, respectively, the decay and phase of the time varying response model. In order to calculate the time-varying natural frequency and damping, the analytic signal, $\ddot{Q}(t)$, is used:

$$\ddot{Q}(t) = \ddot{q}(t) + i\,\mathcal{H}(\ddot{q}(t)) \tag{10}$$

where $\mathcal{H}$ represents a Hilbert Transform. The decay, $d(t)$, is fit to the natural log of the amplitude of the analytic signal, $d(t) = \ln\left|\ddot{Q}(t)\right|$, and the phase, $\theta(t)$, is fit to the unwrapped angle, $\theta(t) = \arg[\ddot{Q}(t)]$.

The phase of the analytic signal gives the oscillation frequency, so the damped natural frequency was defined as its derivative in [5],

$$\omega_d(t) \triangleq \dot{\theta}(t) \tag{11}$$

which one can readily show gives the desired result for a linear time invariant system. Similar expressions can be found for ω_n and ζ.

$$\omega_n(t) \triangleq \left(\omega_d(t)^2 + \dot{d}^2(t)\right)^{\frac{1}{2}} \tag{12}$$

$$\zeta(t) \triangleq \frac{\dot{d}(t)}{\omega_n(t)} \tag{13}$$

The nonlinear stiffness and damping of each mode can now be evaluated based on changes in damping ratio and frequency with respect to time. The instantaneous damping and frequency can be plotted against velocity and displacement amplitude to bring these parameters into a response based form rather than time based.

It is essential to reduce the signal to a single degree of freedom before completing the above process else the envelope and instantaneous phase will be distorted by interference of other modes. In order to assist the modal filter in eliminating unwanted frequency content, a band-pass filter is applied to the modal response. A forward-backward filter was utilized for this supplemental filter which maintained the timing of the original response signal. A brief sensitivity study was completed to investigate the influences of various passbands on each mode. In this study, passbands were varied from ±10% of the natural frequency to as high as ±50%. For each passband and modal response, the time-varying damping and natural frequency (Equations (12) and (13)) were plotted versus time to determine the consequences of narrower/wider passbands. The objective was to find a passband for each mode that successfully eliminated unwanted frequency content without distorting the damping. For this structure the authors have selected to use a 50% passband for all modes which was robust for every mode when using the SMAC modal filter. Note that the passband used here is not universal and might need modification for a different system.

5 Nonlinear Models

This work compared the capabilities of three different models/methods to capture the nonlinear dynamics of the test object: Iwan, FREEVIB (FV), and Restoring Force Surface (RFS). A brief description of each model is provided in the sub sections below. As mentioned in Section 3.3, only those modes that had a damping change greater than 30% between the low and high-level input tests were modeled as nonlinear.

In order to have a fair comparison of their capabilities, each of the three aforementioned models were parameterized with six parameters to capture the dynamics. This quantity was selected as it matches the number of parameters used in the Iwan model.

5.1 Modal Iwan Model

As discussed in [5] and [7] each mode can be modeled with a single degree of freedom system as a modal coordinate. Each modal degree of freedom will be linked to ground with a linear spring and damper. In order to capture the nonlinearity in each mode we then add a four parameter Iwan element in parallel with the linear spring and damper. This element can be described as a joint force as shown in Figure 8.

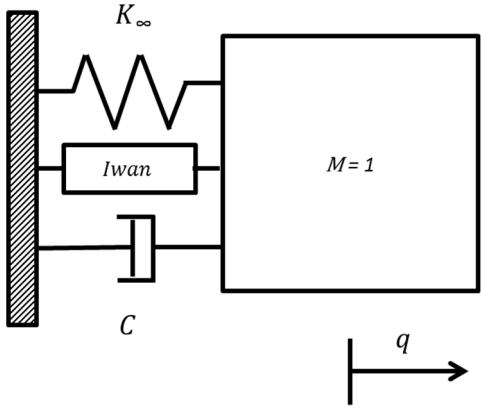

Figure 8 - Schematic of SDOF for Iwan Model modal coordinate

The system is very similar to a standard modal coordinate set-up but with the nonlinear joint force adding complexity due to the nonlinearity of each mode. The equation of motion for the system now takes the form of

$$\ddot{q}(t) + C\dot{q}(t) + K_\infty q(t) = \boldsymbol{\Phi}^T F_{ext} + F_j \tag{14}$$

where the nonlinear force in the joint, F_j, is a function of four parameters, $[F_S, K_T, \chi, \beta]$. F_S is the slip force or the force required to begin macro-slip. K_T is the stiffness in the joint related to the nonlinear frequency shift from linear conditions to macro-slip. χ is related to the exponent in a power-law relationship between damping and amplitude in the macro-slip regime.

Finally, β defines the shape of the dissipation curve near the transition from micro to macro-slip. These four parameters can be obtained from experimental measurements as outlined in [5].

In this work data were obtained solely in the linear and micro-slip regimes of response. Thus some of the parameters became more difficult to estimate. The stiffness in the joint, K_T, is defined as the change in stiffness as shown in (15)

$$K_T = \omega_n^2 - (\omega_n - \Delta\omega_n)^2 \tag{15}$$

where ω_n is the natural frequency when the joint is completely stuck and $\Delta\omega_n$ is the shift in natural frequency when the joint is in macro-slip. Our experiment did not reach macro-slip so this can be used as a bound knowing that $\Delta\omega_n$ must be larger than that seen in the experiment or the results will prove dissatisfactory.

The parameter χ can be determined directly from the damping ratio versus velocity amplitude curve. χ defines the power law exponent on the dissipation versus velocity amplitude curve. In Figure 9 the blue curve shows the measured damping ratio calculated using (13) from the Hilbert Transform. Using this curve one must then subtract off the linear damping ratio (depicted in magenta) from the measured curve. This removes the linear damping portion from the damping ratio and leaves just the nonlinear contribution. This curve can then be fit on a log-log scale in order to determine the slope which is equal to $\chi+1$.

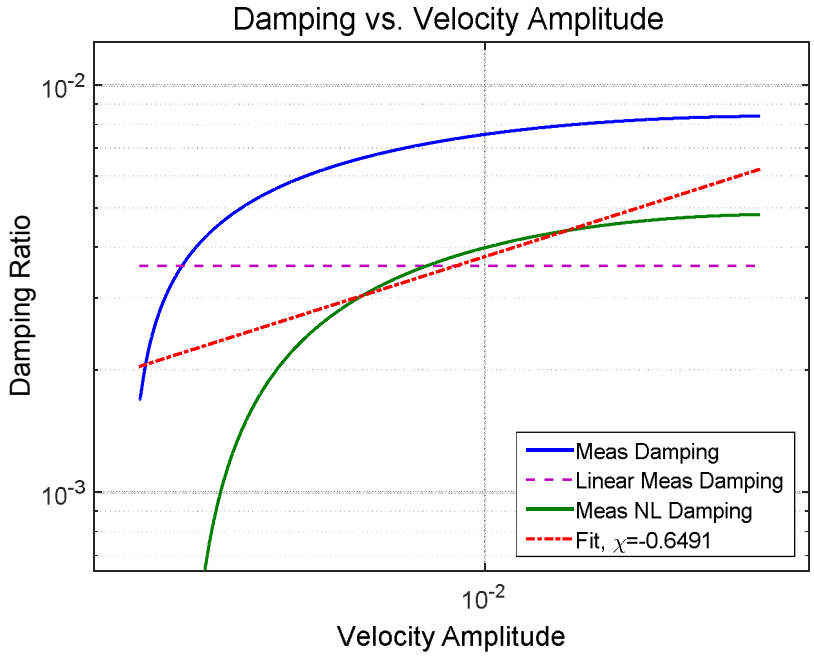

Figure 9 – Damping Ratio versus Velocity Amplitude – Mode 7

As discussed in [8] the damping ratio is fit to the form of (16). C_{zt} is calculated as the intercept of the power law fit from Figure 9.

$$\zeta(\dot{q}) = C_{zt}|\dot{q}|^{\chi+1} \tag{16}$$

In [7], Segalman defines dissipation in a similar form as shown in (17).

$$Dissipation = R|q|^{\chi+3} \tag{17}$$

In Ginsberg's text [9], the relationship between damping ratio and dissipation can be used to solve for the coefficient R.

$$\zeta = \frac{Dissipation}{m2\pi\omega_d\omega_n|q|^{\chi+3}} \tag{18}$$

(19)

$$R = C_{zt} 2\pi \omega_d^{\chi+2} \omega_n$$

Based on additional 4-parameter Iwan model definition from [7] one can solve for the remaining unknown parameters β and F_S using an assumed K_T along with extracted values for χ and R. Using these 4-parameters the joint force can now be calculated and integrated. The identification procedure described above was performed on the nonlinear modes specified in Section 3.3 and the results are provided in Table 4 below.

Table 3 – Modal Iwan Model Parameters

Mode	χ	β	F_S	K_T	$f_{n,lin}$	ζ_{lin}
7	-0.65	0	245	2.10E+05	119	0.0036
8	-0.31	0	39	2.91E+05	160	0.0021
9	-0.22	0	51	9.92E+05	276	0.0246
12	-0.77	0	52	9.69E+05	503	0.0067
13	-0.79	0	108	2.24E+06	592	0.0202

5.2 FREEVIB

This nonlinear model was developed by Feldman in [10] and bases its theory on the free vibration of a nonlinear system. Unlike the Iwan model, FREEVIB combines the linear and nonlinear restoring elements as seen in Figure 10**.**

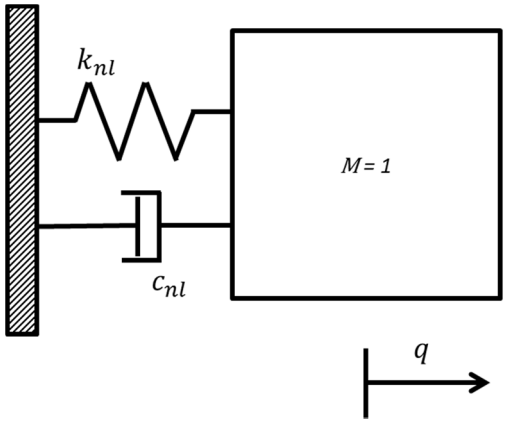

Figure 10 - Schematic of SDOF for FV modal coordinate

The governing equation of motion is in the following form:

$$\ddot{q}(t) + 2c(A_q)\dot{q}(t) + k(A_q)q(t) = 0 \tag{20}$$

where c and k are the instantaneous damping and stiffness coefficients as a function of amplitude, A_q, which is the Hilbert envelope of the displacement. Note that, using the nomenclature from Section 4.2, $A_q = e^{d(t)}$. With the assumption that $c(A_q)$ and $k(A_q)$ vary slowly, the Hilbert Transform is utilized to create (20) in terms of the analytic signal of $q(t)$, i.e.,

$$\ddot{Q}(t) + 2c(A_q)\dot{Q}(t) + k(A_q)Q(t) = 0 \tag{21}$$

where $\ddot{Q}(t)$ comes from (10). Given that the 1st and 2nd derivatives of the analytic signal can be written in terms of $Q(t)$, the envelope, and instantaneous phase, a closed-form, nonparametric function can be derived for c and k. Using the definitions for the envelope and instantaneous phase from Section 4.2 and ignoring negligibly small terms, the instantaneous damping and stiffness terms are determined to be:

$$c(t) = -\dot{d}(t) - \frac{\dot{\omega}_d(t)}{2\omega_d(t)} \tag{22}$$

$$k(t) = {\omega_d}^2(t) \tag{23}$$

where $\omega_d(t)$ is the instantaneous damped natural frequency defined in (11).

Typically, damping is associated with velocity and therefore it is desired to derive an expression for c in terms of velocity. If small terms are neglected, the velocity envelope, $A_{\dot{q}}$, can be written as

$$A_{\dot{q}} = \omega_d A_q. \tag{24}$$

Now $c(t)$ and $k(t)$ can be plotted against $A_{\dot{q}}(t)$ and $A_q(t)$, respectively, to get amplitude-dependent instantaneous damping and stiffness coefficients. For the work described herein, it was desired to have all nonlinear models utilize the same number of parameters. Therefore, instead of conducting the nonlinearity identification step described in [10], the stiffness and damping were estimated using quadratic polynomials (resulting in linear, quadratic, and cubic terms in the equation of motion).

$$c\left(A_{\dot{q}}\right) = c_0 + c_1 A_{\dot{q}} + c_2 A_{\dot{q}}^2 \tag{25}$$

$$k\left(A_q\right) = k_0 + k_1 A_q + k_2 A_q^2 \tag{26}$$

When implementing FREEVIB in simulation, we calculated the instantaneous damping and stiffness as:

$$c(\dot{q}_i) = c_0 + c_1|\dot{q}_i| + c_2 \dot{q}_i{}^2 \tag{27}$$

$$k(q_i) = k_0 + k_1|q_i| + k_2 q_i{}^2 \tag{28}$$

where q_i and $\dot{q}_i$ are the displacement and velocity at time step i. The absolute values are used to preserve the sign of the signal.

FREEVIB requires that the data used in the nonlinear parameter identification can only include the response after the excitation is removed. Since the measured force was filtered and never reached a value of identically zero, this was approximated as when the filtered force had dropped below 0.5% of its maximum value. Depending on the post-processing and degree of nonlinearity of the measurements, a significant amount of time may have elapsed prior to this event occurring. This could result in the exclusion of a significant portion of the nonlinear response from the analysis, reducing the accuracy of the extracted parameters. This effect can be seen in the results for mode 9.

The identification procedure described above was performed on the nonlinear modes specified in Section 3.3 and the results are provided in Table 4 below.

Table 4 - FREEVIB Damping and Stiffness Coefficients

Mode	c_2	c_1	c_0	k_2	k_1	k_0
7	-6.12E+03	301	2	2.08E+13	-1.77E+09	5.60E+05
8	-1.01E+04	454	0.43	2.63E+13	-1.98E+09	1.01E+06
9	-1.49E+06	1.15E+04	39	-2.29E+16	1.49E+11	2.79E+06
12	-144	30	24	6.91E+13	-1.04E+10	9.80E+06
13	4.57E+04	-1.96E+03	95	-1.87E+15	-1.53E+10	1.31E+07

5.3 Restoring Force Surface

This method has been extensively researched and refined with several permutations. Reference [11] contains an extensive synopsis of the past variances and applications of the Restoring Force Surface (RFS) method. Similar to the Iwan model, the version of the RFS model structure adopted for this work is shown in Figure 11 where the linear elements are in parallel with the nonlinear ones.

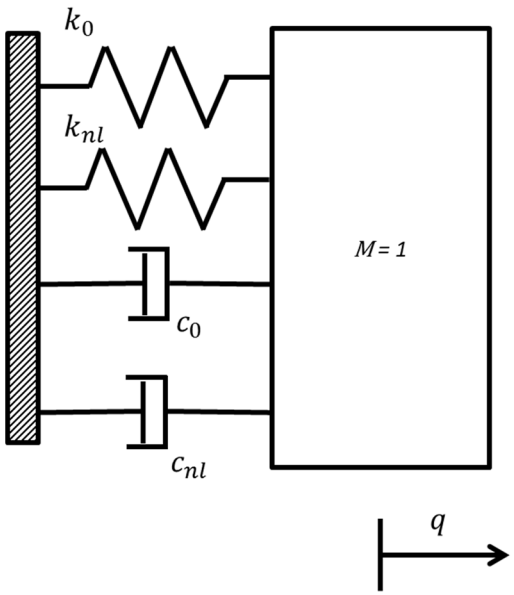

Figure 11 - Schematic of SDOF for RFS modal coordinate

The foundation of RFS is in the Newtonian equation of motion:

$$\ddot{q}(t) + F_r(q(t), \dot{q}(t)) = F(t) \tag{29}$$

where $F_r(q, \dot{q})$ represents the damping and stiffness forces (called the restoring forces) and $F(t)$ is the excitation force. Assuming the acceleration and excitation force are measured, then at every time instant, the restoring force is also known. We write F_r as in the following:

$$F_r(q(t), \dot{q}(t)) = c_0\dot{q}(t) + c_1|\dot{q}(t)|\dot{q}(t) + c_2\dot{q}^3(t) + k_0q(t) + k_1|q(t)|q(t) + k_2q^3(t) \tag{30}$$

where $c_1, c_2, k_1,$ and k_2 are constants. Since c_0 and k_0 are already known from the low level modal tests, (29) is rearranged to

$$[|\dot{q}|\dot{q} \quad \dot{q}^3 \quad |q|q \quad q^3] \begin{bmatrix} c_1 \\ c_2 \\ k_1 \\ k_2 \end{bmatrix} = F - \ddot{q} - c_0\dot{q} - k_0q \tag{31}$$

or

$$[P] \begin{bmatrix} c_1 \\ c_2 \\ k_1 \\ k_2 \end{bmatrix} = [U] \tag{32}$$

where the time-dependency associated with each row has been omitted for clarity. Recall that $[P]$ and $[U]$ are processed measurements and that there is a row for each time sample. Thus (32) should be written as

$$\mathbf{P} \begin{bmatrix} c_1 \\ c_2 \\ k_1 \\ k_2 \end{bmatrix} = \bar{\mathbf{U}}. \tag{33}$$

We obtained the best results by taking the Fourier transform of each column of P and U giving

$$\mathbf{P}_{\mathcal{F}} \begin{bmatrix} c_1 \\ c_2 \\ k_1 \\ k_2 \end{bmatrix} = \bar{\mathbf{U}}_{\mathcal{F}}. \tag{34}$$

Note that in order to yield real coefficients, $\mathbf{P}_{\mathcal{F}}$ must be reconfigured to

$$\mathbf{P}_{\mathcal{F}} = \begin{bmatrix} real(\mathbf{P}_{\mathcal{F}}) \\ imaginary(\mathbf{P}_{\mathcal{F}}) \end{bmatrix}. \tag{35}$$

$\bar{\mathbf{U}}_{\mathcal{F}}$ must be similarly restructured. Pre-multiplying $\bar{\mathbf{U}}_{\mathcal{F}}$ by the pseudo-inverse of $\mathbf{P}_{\mathcal{F}}$ results in the least-squares estimate for $c_1, c_2, k_1,$ and k_2.

We obtained good results by applying a weighting matrix to (34) near resonances. If the weighted bandwidth is taken to be ±5% of the frequency of the resonance, this method gave better parameters than the time domain results from (33).

$$\mathbf{W}\mathbf{P}_{\mathcal{F}} \begin{bmatrix} c_1 \\ c_2 \\ k_1 \\ k_2 \end{bmatrix} = \mathbf{W}\bar{\mathbf{U}}_{\mathcal{F}} \tag{36}$$

where $\mathbf{W}$ is the block diagonal weighting matrix. For the Restoring Force Surface results in Section 6.1, this weighted frequency domain approach was utilized with a weight of 100 applied to the narrow resonance bands and 1 elsewhere.

Note that acceleration, velocity, and displacement must all be known (estimated or measured). For this work, acceleration was obtained from the modal filtered measured accelerations and the other two states were estimated by integrating in the frequency domain. The first step was to band-pass filter the modal acceleration as prescribed in Section 4.2. The velocity and displacement in the frequency domain were then calculated by dividing this acceleration by $i\omega$ and $-\omega^2$, respectively, followed by band-pass filtering using the same filter that was applied to the modal acceleration.

The identification procedure described above was performed on the five nonlinear modes, and the results are provided in Table 5.

Table 5 - Restoring Force Surface Damping and Stiffness Coefficients

Mode	c_2	c_1	c_0	k_2	k_1	k_0
7	-1.36E+03	367	5	1.69E+13	-1.5E+09	5.56E+05
8	-3.77E+03	579	4	1.52E+13	-1.8E+09	1.01E+06
9	-1.94E+05	6.63E+03	85	6.14E+14	-1.5E+10	3.01E+06
12	-5.35E+02	299	42	1.49E+14	-1.9E+10	1.00E+07
13	-3.24E+04	3.33E+03	150	4.42E+15	-1.6E+11	1.38E+07

6 Results and Observations

This section compares the results of each of the three nonlinear modal models to the actual nonlinear measured data. First, a discussion of the simulations used to create the analytical modal responses for linear and nonlinear modes is presented followed by a comparison to measured data in physical coordinates. Discussions of features of each method will conclude this section.

6.1 Simulation Results and Observations

The three pseudo-modal models with 17 modes were excited with simulated modal forces corresponding to the measured high level impacts from the three different locations. The modal responses were extended to the physical dof using the linear mode shape matrix extracted from low level modal tests using (4). These responses were compared against the measured

high level data in the plots below. Note that the line labeled “Linear” is the response of a linear model that used the low-level linear parameters from Table 2 for all 17 modes.

A representative sample of results are presented. Figure 12 compares the linear model response with the measured data by considering the primary singular value of the complex mode indicator function (CMIF). The CMIF compresses all the responses from all three force impacts into one plot. This plot illustrates that the linear model over-predicts the response from a high level impact; the three main modes of the system (7, 8, and 12) are over-predicted by almost 100%. Additionally, the linear model is slightly too stiff.

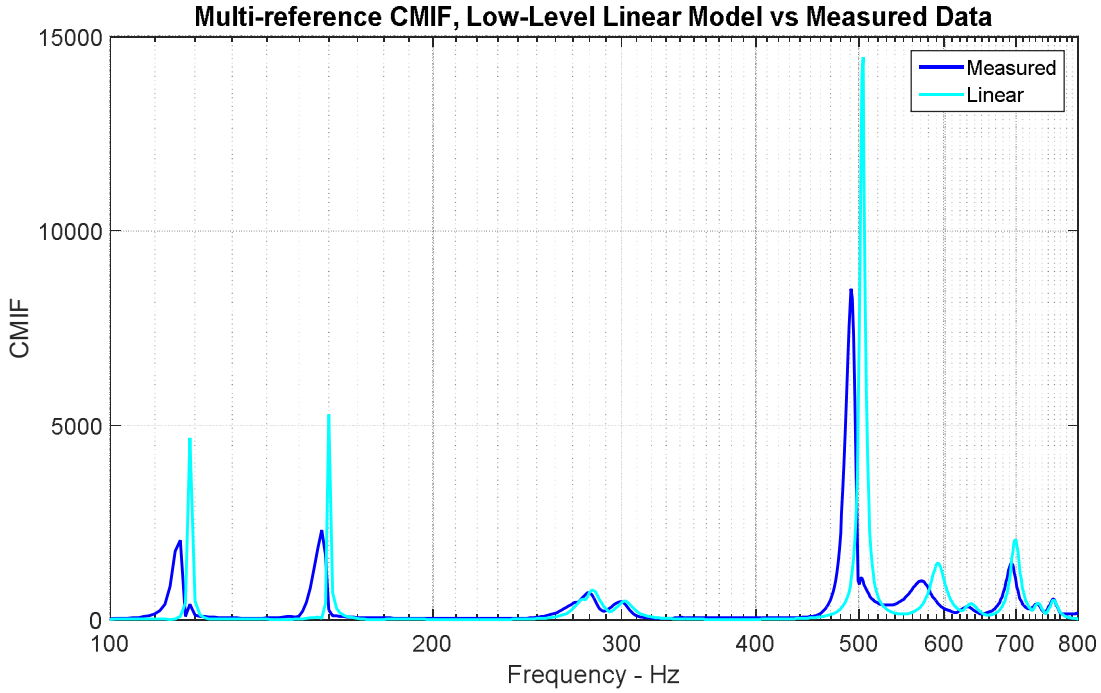

Figure 12 - Multi-reference CMIF, linear model versus measured data, max singular value only

Figure 13 shows the primary singular value of the multi-reference CMIF of the high-level measured data and the corresponding predictions of the three nonlinear models. All models are able to predict the high-level test data better than the linear model, with the exception of FV’s 273 Hz response. Only the Iwan and RFS models will be addressed further, since the FV model over-predicts two modes. Note that for declared linear modes, the three model results overlay, an expected result since all three pseudo-modal models were the same for the linear modes.

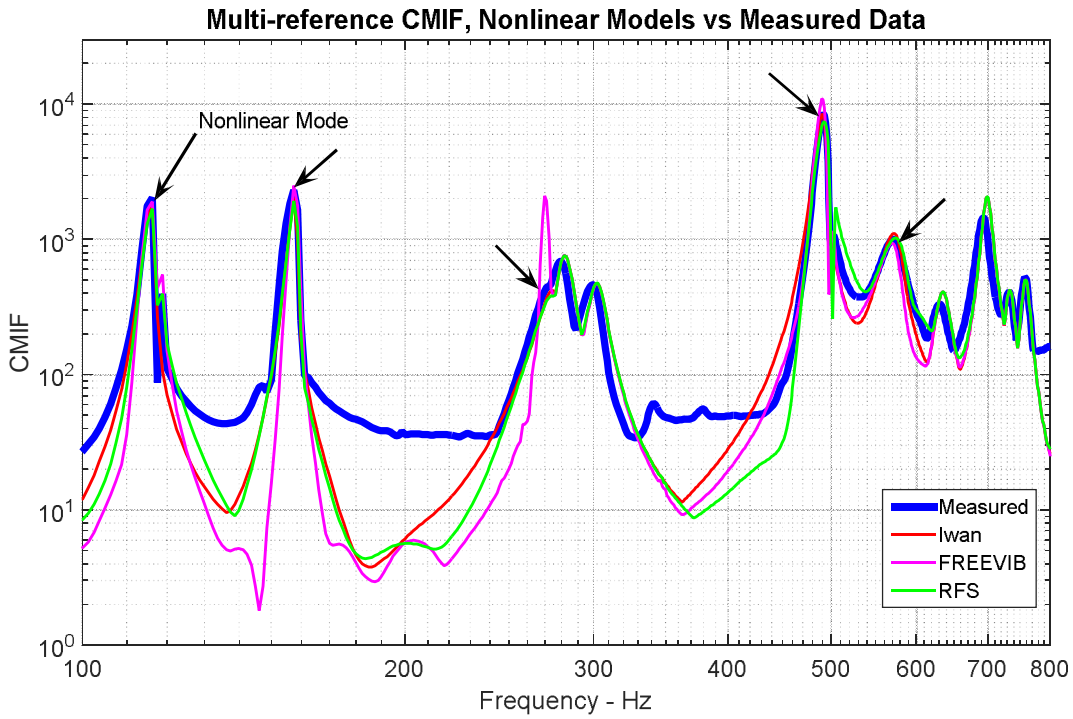

Figure 13 - Multi-reference CMIF, nonlinear models versus measured data, max singular value only

The time history plots of Figure 14 through Figure 17 reinforce the results from Figure 13. The drive point response to the axial input (Figure 14 and Figure 15) is dominated by mode 12. The Iwan model was able to accurately replicate the measured data in Figure 13, and there is a good agreement in the time response shown in Figure 14. Results are similar for the RFS approach with cubic springs and dampers in Figure 15.

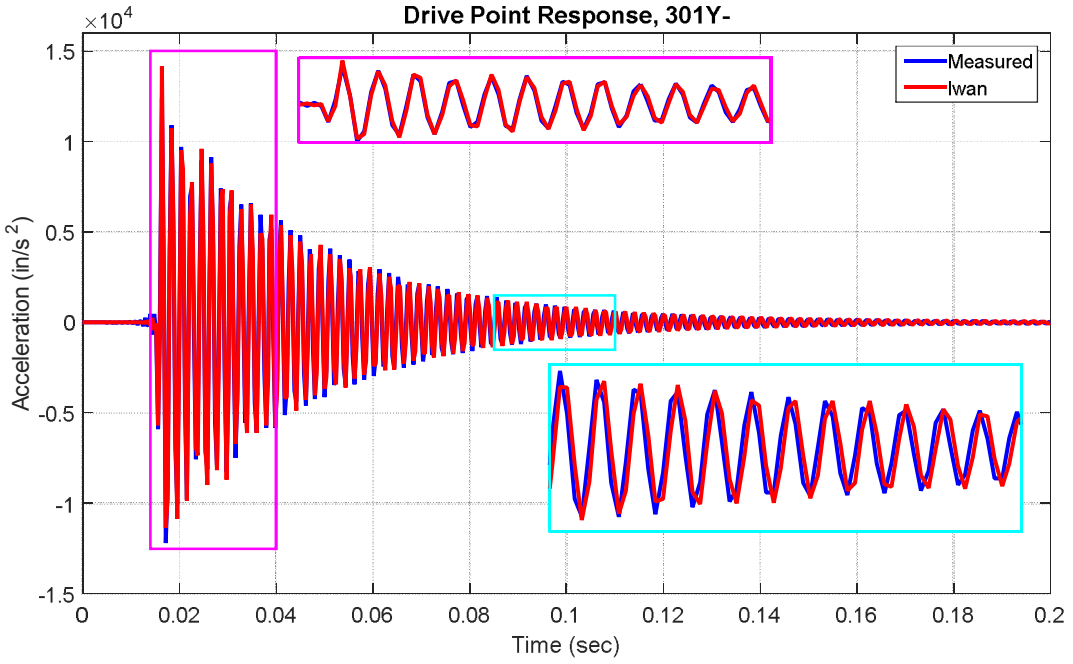

Figure 14 - Axial drive point response, Iwan versus measured

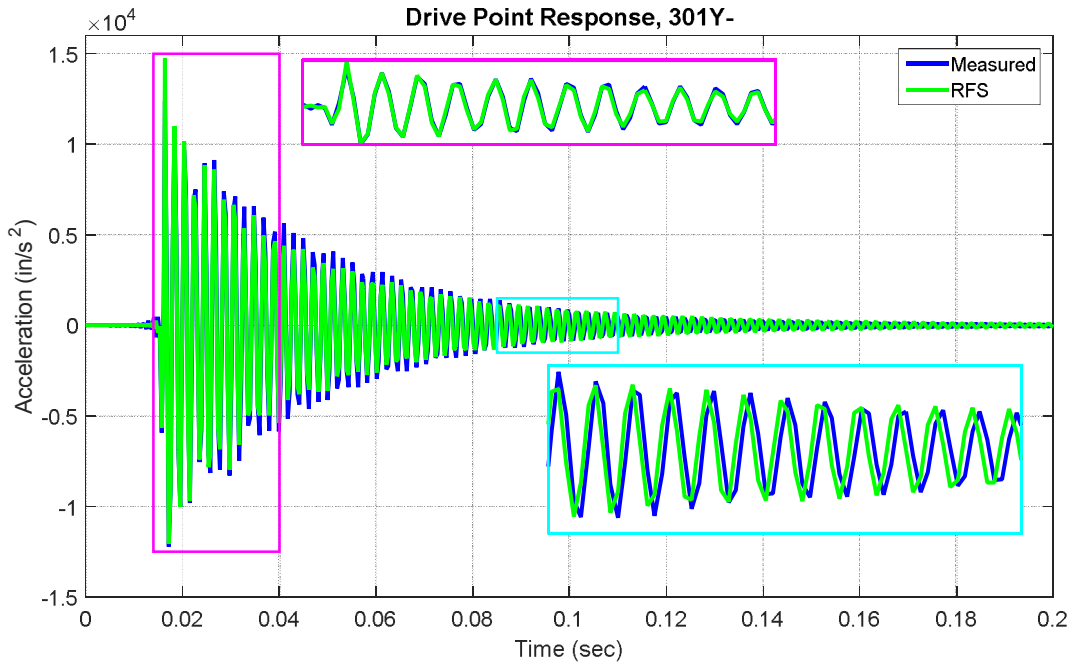

Figure 15 - Axial drive point response, RFS versus measured

The Iwan and RFS models comparably predicted the drive point response from the radial input in Figure 16 and Figure 17. Neither achieved the proper amplitude of the initial acceleration spike, but they simulate the rest of the time history well.

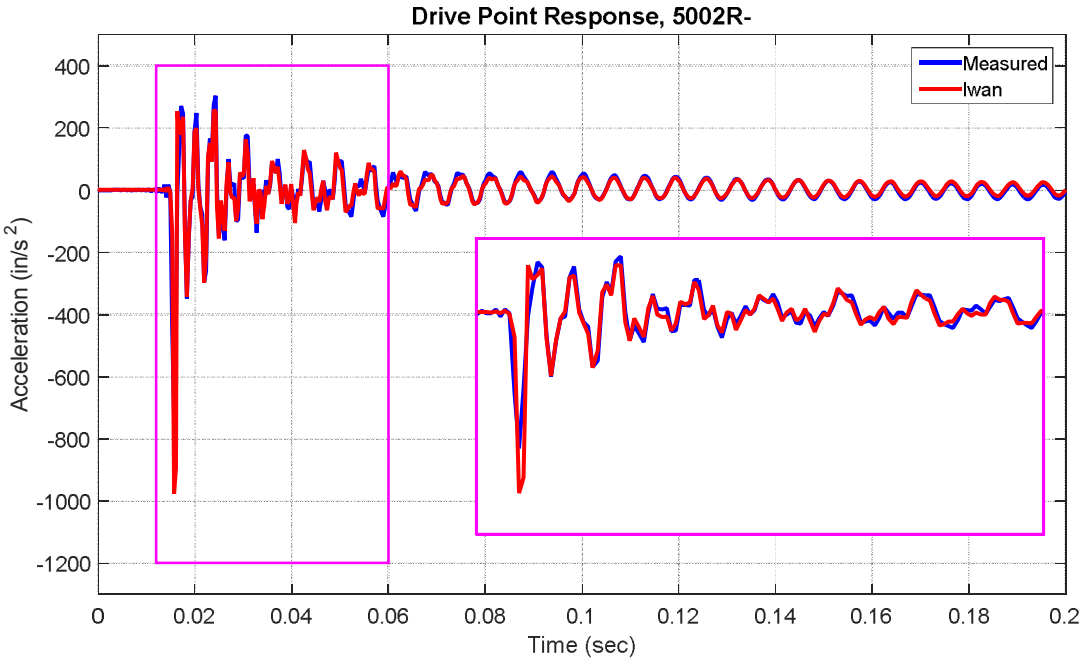

Figure 16 - Radial drive point response, Iwan versus measured

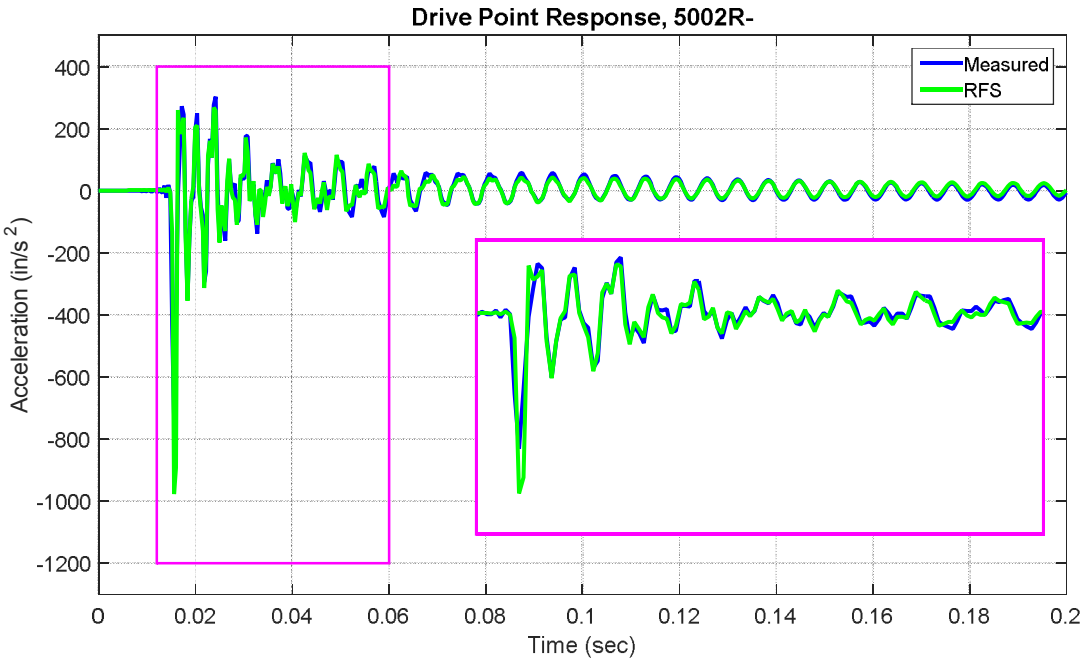

Figure 17 - Radial drive point response, RFS versus measured

6.2 Discussion

Although not readily apparent from the figures, it is important to note the significant role of the Hilbert Transform in the Iwan and FV models. While an extremely valuable and versatile tool that provides great qualitative insight into the frequency and damping variation, it can also have adverse effects depending on the characteristics of the data. In the presence of step changes in signal amplitude or frequency, the envelope and instantaneous phase produced by the Hilbert Transform will have some overshoot and settling time characteristics [12]. Given that this work utilized impact data which has a large step-like change in amplitude, the envelopes and instantaneous phases extracted from the Hilbert Transform of the measured data were distorted during the initial portion of the response. These errors consequently influenced the polynomial fits for the envelope and instantaneous phase upon which the Iwan and FV models depend.

Another aspect worth mentioning is the interplay of the Hilbert Transform and the quality of the modal filter. In addition to the transient effects mentioned above, any non-targeted modal peaks that are not adequately attenuated in the modally-filtered response can produce ripples throughout the entire envelope. These ripples influence the polynomial fits to the Hilbert Transform and hence the nonlinear parameters of the Iwan and FV models. In extreme cases when the modal filter cannot eliminate a nearby mode (e.g. mode 9), the envelope and instantaneous frequency (and hence the nonlinear parameters) are distorted by the non-suppressed mode. This phenomenon contributed to the inaccurate response of mode 9 predicted by FV, see Figure 13. Note that FV results could be improved with user interaction, see Section 7.4. The Iwan model avoids these struggles with mode 9 because the Iwan element is placed in parallel with a known linear spring and damper. Rather than letting the Hilbert transform fit these linear terms the Iwan element is constrained to be in a reasonable range when the parameters are being determined. The RFS method can also suffer from non-targeted poorly attenuated modal peaks in the modally-filtered response, but does not rely on the Hilbert Transform, which eliminates effects from the Hilbert distortions as well as the extra steps of calculating and fitting the Hilbert Transform.

As one can see from Figure 9, the process for subtracting the linear damping and fitting a line to the log plot of damping vs amplitude are not completely straight-forward. Significant trial-and-error was required to iterate to the final high quality solutions that were achieved.

7 Conclusions

The conclusions here will address the model assumptions, test approach, signal pre-processing and the three nonlinear models.

7.1 Nonlinear Pseudo-modal Model Assumptions

The assumptions that the mode shapes do not change and that the modal degrees of freedom do not interact appear valid to a reasonable approximation for this hardware testing. The hardware showed the typical structural dynamic nonlinearity of softening spring and increasing damping with amplitude for at least five modes. Other modes were considered linear enough that they were approximated as linear. No modes exhibited the hardening spring effect that is occasionally seen in some hardware.

7.2 Nonlinear Pseudo-modal Model Testing Approach

The testing approach included a low level impact modal test to obtain the normal linear modal parameters from three input locations. The key effort here was to provide as perfect as possible co-linear force input with the driving point accelerometer so that the linear experimental modal model is extracted with accurate modal mass and accurate mode shapes scaling. The low level modal test is a very standard test in the industry and quite tractable for most laboratories. The high level impact is just a repeat of the low level test at higher levels, and does not require much extra effort once the test is set up. Some care is required to make sure the sensors do not overload and corrupt the data. The maximum response capability of the drive point accelerometer was a limiting factor in this test.

7.3 Signal pre-processing with modal filter, band pass filter and Hilbert Transform

The quality of the modal filtering has a direct impact on the quality of the nonlinear parameter identification for all three nonlinear model forms. When one observes the modal filtered signal in the frequency domain, one can usually discern with the eye whether modes at other frequencies have been removed. Nonlinear parameter results tend to be very good with a sdof modal filtered response and worse as more modes are observed in the supposedly filtered response.

The full modal filter and the SMAC modal filter each had certain modes on which they excelled. The SMAC modal filter was better at removing extra modes than the full modal filter in general. The single modal filter was much worse than the other two.

Band-pass filtering was very helpful for improving the Hilbert Transform results. Without band-pass filtering the Hilbert Transform results were much more oscillatory and nebulous, usually due to other modes that were not completely filtered. Band-pass filtering was not helpful if the pass band was too narrow (e.g. five percent of the resonant frequency). It could be tailored to each mode for optimum results, but generally a band-pass of 30-50 percent of the resonant frequency was robust. The Hilbert Transform is required for the FREEVIB and Iwan approaches to obtain frequency and damping variation as a function of amplitude. If the modal filtered response was not uni-modal, these functions of frequency and damping were oscillatory, hampering the fitting. The Hilbert Transform tends to have some early-time oscillations of frequency and damping at the very high amplitudes. The spurious oscillations at the high amplitude can be problematic, since that is the region most important to the nonlinear model.

7.4 Nonlinear pseudo-modal model forms

We contend that all three methods would give satisfactory nonlinear simulations with enough user interaction. For these studies, the Iwan model and the RFS frequency fit model gave satisfying simulation results. The FV model was not quite as good, but with some user interaction these results could be improved. We did not iterate on the FV fits near as much as the Iwan fits. Six parameters were chosen for each mode for each method to put them on equal footing. This was initially based on the Iwan approach, which uses a linear spring and damper and a four parameter Iwan. With this many parameters, any of the model forms could be used for this nonlinear hardware.

The Iwan model is the most utilized in simulating structural dynamic joint nonlinearities in the recent past. Its form appeared to be a very good representation for the nonlinearities where damping increased and frequency decreased with amplitude, which seems to be typical of many joints. We considered the simulations with the Iwan models very good. The disadvantages we noted with the Iwan were: 1. a great deal of user interaction (and iteration) was required to get good Iwan parameters; 2. the understanding of those parameters is complex compared to FREEVIB stiffness and damping or cubic springs and damping; 3. the inability to simulate constant damping with softening or decreased damping with stiffening; 4. a strong dependence on the quality of the Hilbert Transform results.

The Feldman FREEVIB model is relatively easy to understand. We modified the nonparametric approach by fitting cubic polynomials to the functions of frequency and damping vs. amplitude to keep it on the same six parameter footing as the other two model forms. FREEVIB requires free response ringdown data, which works well with impact testing as was performed on this hardware. Simulation results are very dependent on the results of the Hilbert Transform and the modal filter. We found that parameters for mode 9 were not well quantified using FV , causing significant over-prediction for this mode. However, if we removed the band-pass filtering which allowed us to include earlier time data while still maintaining

the free-vibration requirement, we could get better results. Additionally, using the FMF (which performed better for mode 9, see Figure 7) instead of the SMAC modal filter for this particular mode also resulted in a better prediction of the measured data . We surmise that capturing the most nonlinear response early in time and eliminating non-target modes is critically important to FV. We did not include the improved results since the data processing (different modal filter and/or exclusion of band pass filtering) was inconsistent with the other two nonlinear models.
The cubic springs and dampers as a function of amplitude are easy for an engineer to understand. The RFS approach in the frequency domain focused on the frequency lines around each resonance gave results on par with the best results from iterative Iwan fits. The RFS frequency approach also has other significant advantages over the other models because it does not require the Hilbert Transform or extensive user interaction. Because of the ease of understanding the polynomial type nonlinearity, elimination of Hilbert Transform step, low user interaction and the final quality of the nonlinear simulation, RFS with cubic nonlinearities emerged as our favored approach.

8 References

[1] Segalman, D.J., A Modal Approach to Modeling Spatially Distributed Vibration Energy Dissipation", Sandia National Laboratories, Albuquerque, NM and Livermore, CA, SAND2010-4763, 2010.

[2] Deaner, Brandon, J., "Modeling the Nonlinear Damping of Jointed Structures Using Modal Models," Master of Science Thesis, University of Wisconsin-Madison, 2013.

[3] Hensley, Daniel P., Mayes, Randy L., "Extending SMAC to Multiple References", Proceedings of the 24th International Modal Analysis Conference, pp 220-230, January 2006

[4] Mayes, R.L. and Johansen, D.D. "A Modal Parameter Extraction Algorithm Using Best-Fit Reciprocal Vectors", Proceedings of the 16th International Modal Analysis Conference, pp 517-521, February 1998.

[5] B. Deaner, Allen, M. S., Starr, M.J., Segalman, D.J., and Sumali, H., "Application of Viscous and Iwan Modal Damping Models to Experimental Measurements From Bolted Structures," *ASME Journal of Vibration and Acoustics,* vol. 137, 2015 2015.

[6] M. W. Sracic*, et al.*, "Identifying the modal properties of nonlinear structures using measured free response time histories from a scanning laser Doppler vibrometer," presented at the 30th International Modal Analysis Conference Jacksonville, Florida, 2012.

[7] D. J. Segalman, "A Four-Parameter Iwan Model for Lap-Type Joints," Journal of Applied Mechanics, vol. 72, pp. 752-760, September 2005.

[8] D. R. Roettgen and M. S. Allen, "Nonlinear characterization of a bolted, industrial structure using a modal framework," *Submitted to Mechanical Systems and Signal Processing*, 2015.

[9] J. H. Ginsberg, *Mechanical and Structural Vibrations*, First ed. New York: John Wiley and Sons, 2001.

[10] Feldman, M. "Non-Linear System Vibration Analysis Using Hilbert Transform—I. Free Vibration Analysis Method 'FREEVIB'", *Mechanical Systems and Signal Processing*, 1994 Vol 8, pp119-127.

[11] Gaëtan, K., Worden, K., Vakakisc F. A., Golinval, J.C., "Past Present, and Future of Nonlinear System Identification in Structural Dynamics," *Mechanical Systems and Signal Processing*, 2006, Vol 20, pp505-592.

[12] Feldman, M., 2011, *Hilbert Transform Applications in Mechanical Vibration* (John Wiley & Sons, Ltd.), pp29